Identification of combined sensor faults in structural health monitoring systems

Heba Al-Nasser, Thamer Al-Zuriqat, Kosmas Dragos, Carlos Chillón Geck, and Kay Smarsly

Hamburg University of Technology, Institute of Digital and Autonomous Construction, Blohmstraße 15, 21079 Hamburg, Germany

Abstract

Fault diagnosis (FD), comprising fault detection, isolation, identification and accommodation, enables structural health monitoring (SHM) systems to operate reliably by allowing timely rectification of sensor faults that may cause data corruption or loss. Although sensor fault identification is scarce in FD of SHM systems, recent FD methods have included fault identification assuming one sensor fault at a time. However, real-world SHM systems may include combined faults that simultaneously affect individual sensors. This paper presents a methodology for identifying combined sensor faults occurring simultaneously in individual sensors. To improve the quality of FD and comprehend the causes leading to sensor faults, the identification of combined sensor faults (ICSF) methodology is based on a formal classification of the types of combined sensor faults. Specifically, the ICSF methodology builds upon long short-term memory networks, i.e. a type of recurrent neural networks, used for classifying "sequences", such as sets of acceleration measurements. The ICSF methodology is validated using real-world acceleration measurements from an SHM system installed on a bridge, demonstrating the capability of the long short-term memory networks in identifying combined sensor faults, thus improving the quality of FD in SHM systems. Future research aims to decentralize the ICSF methodology and to reformulate the classification models in a mathematical form with an explanation interface, using explainable artificial intelligence, for increased transparency.

Keywords: Identification of combined sensor faults (ICSF), sensor faults, fault diagnosis (FD), structural health monitoring (SHM), classification models, long short-term memory (LSTM) networks.

1. Introduction

As a non-destructive evaluation technique, structural health monitoring (SHM) utilizes sensor data to evaluate and assess structural conditions (Law et al., 2014). SHM systems provide continuous updates on the structural conditions, ensuring both safety and cost-efficient maintenance of the structures being monitored (Liu and Nayak, 2012). SHM relies on sensors operating continuously over long periods of time to collect sensor data used for structural assessment (Dong and Catbas, 2021). Exposure to aging, degradation, and harsh environmental conditions may lead to sensor faults in SHM systems (Smarsly and Law, 2014). Undiagnosed sensor faults may cause system malfunctions and even system failures, highlighting the importance of fault diagnosis (FD) in SHM systems, which includes fault detection, isolation, identification, and accommodation (Patton, 1990).

Fault detection aims to capture faults in SHM systems, fault isolation entails the localization of faults, fault identification involves determining fault types, and fault accommodation represents the compensation for the effects of faults. Sensor fault types, depending on the classification schema, include bias, drift, gain, precision degradation, complete failure (Dragos and Smarsly, 2016), and outliers (Dervilis et al., 2016). FD in SHM systems has been a matter of increasing importance in research over the past decades (Steiner et al., 2019), with most approaches being based on physical or analytical redundancy. In physical redundancy, "redundant" sensors are installed next to the sensors of an SHM system. Then, data recoded by the redundant sensors is compared with data recorded by the sensors of the SHM system, and the results of the comparison are used for fault diagnosis. To reduce the cost and power consumption associated with the relatively large number of sensors required in physical redundancy approaches, analytical redundancy uses mathematical models and redundant information inherent to the sensor data recorded by the SHM systems, for estimating "virtual" outputs. Faults are diagnosed on the basis of residuals between virtual outputs and actual sensor data, representing a concept that is well established in several engineering disciplines since many years (Isermann and Ballé, 1997).

The emphasis of most FD approaches in the past decades centers around detecting, isolating, and accommodating sensor faults, without considering fault identification. Kullaa (2007) has introduced a detection, isolation, and accommodation method for sensor faults in SHM systems. A method has been proposed by Smarsly and Petryna (2014) for decentralized fault detection in wireless SHM systems, based on analytical redundancy in sensor data in the time domain, using multi-layer backpropagation feedforward neural networks. The aforementioned method has been extended to use frequency-domain data by Dragos et al. (2016). Huang et al. (2017) have proposed a method for detecting and isolating sensor faults in wireless SHM systems using weighted principal component analysis. A method based on support vector regression has been reported by Steiner et al. (2019) for decentralized detection and

isolation of sensor faults. Giordano et al. (2023) have explored incorporating sensor validation tools to provide information on the actual condition of sensors in SHM systems, extending the value of information from the Bayesian decision theory to quantify the information on the condition of the sensors to decision-making. Deng et al. (2023) have reported a review about sensor fault detection methods in SHM, providing the advantages, disadvantages, and scope of the method investigated. However, in the aforementioned studies fault identification has been overlooked, despite its importance for improving the quality of FD as well as for gaining insights into underlying causes of sensor faults in SHM systems. The main reason for neglecting fault identification is the need for complex models, which increase the computational burden of FD. Nevertheless, a few studies that consider fault identification in SHM have been reported. For example, Yu et al. (2014) have proposed rough set theory and a support vector machine (SVM) network for identifying sensor faults. Fritz et al. (2022) have introduced a fault identification method for SHM systems using wavelet-transformed sensor data, deployed as input to a convolutional neural network (CNN) that classifies single sensor faults. Oncescu and Cicirello (2022) have presented a classification model for sensor fault identification using natural language processing for extracting fault labels from failure reports, along with Naiive Bayes, SVM, and artificial neural networks for identifying faults in sensors exhibiting multiple fault types occurring at different time instances. A CNN-based 3-channel imagery approach has been reported by Shajihan et al. (2022) for sensor fault identification, comprising time histories, histograms, and probability density function representations of sensor data. Luo et al. (2023) have reported a structural damage identification approach considering sensor faults aiming to identify types of structural damage and sensor faults occurring separately or simultaneously. Mou et al. (2022) have introduced a 2-D CNN-based approach for fault identification in strain gauges for offshore SHM, considering bias, gain, and complete failure. Nong et al. (2023) have reported sensor fault identification using a multimodal deep neural network consisting of 1D and 2D CNN channels. Pan et al. (2023) have presented a transfer-learning-based approach for sensor fault identification using convolutional neural networks. In bridge SHM, Guo (2023) has proposed an approach for sensor fault identification combining 1D CNN with LSTM. Li et al. (2023a) have introduced sensor fault diagnosis strategy using a deep CNN model enhanced with data augmentation, based on two stages, a sensor fault detection stage followed by a sensor fault identification stage.

Representing common ground among fault identification studies for SHM systems found in literature, single faults are assumed in the majority of the studies. However, SHM systems may exhibit “combined sensor faults”, i.e., combinations of two or more faults occurring simultaneously in data recoded by individual sensors. For example, combined sensor faults have been reported as an incidental observation during experimentation, specifically in the form of gain and linear drift faults occurring in sensors when transmission cables are deliberately bent (Li et al., 2023b). To the knowledge of the authors, identification of combined sensor faults in SHM systems has hardly been investigated.

Despite the scarce attention received in SHM, sensor fault identification and, in particular, the identification of combined faults has been investigated in other disciplines for more than two decades, as it is an important means to comprehend the causes of sensor faults. A method for detecting, identifying, and accommodating faulty sensors in a boiler process has been proposed by Qin and Li (1999) using structured residuals with maximized sensitivity, where each structured residual is only affected by specific sensor faults. Considering four fault types, i.e. bias, drift, precision degradation, and complete failure, the authors have been able to identify single sensor faults as well as simultaneous faults affecting different sensors. Cheng et al. (2023) have reported on a sensor fault identification method, termed "adaptive particle swarm optimization support vector machine" (APSO-SVM), where APSO optimizes the parameters of the SVM network. The method has been applied to diverse types of sensors deployed in a research lab, proving that APSO-SVM is capable of identifying combined sensor faults that consist of bias and drift. Shen et al. (2024) have proposed a multi-sensor multi-type fault diagnosis method for lithium-ion battery, using a two-layer identification algorithm based on correlation coefficient, impulse factor, and Hurst coefficient to identify specific fault types, i.e. bias, gain, drift, and precision degradation. An "unknown input sliding mode observer" approach has been introduced by Xia et al. (2023) to identify three sensor faults, namely bias, drift, and gain. Luca et al. (2023) have presented a methodology for fault identification of dissolved oxygen sensors in wastewater treatment plants using the Fisher discriminant analysis to identify six sensor fault types, bias, drift, gain, precision degradation, fixed value, and complete failure. In automotive software systems, Abboush et al. (2023) have reported a methodology to identify combined sensor faults using ensemble long short-term memory (LSTM) and random forest networks. In the field of mechatronic systems, Sergiyenko et al. (2022) have introduced an approach for sensor fault identification via linear and nonlinear dynamic models using sliding mode observers. A simultaneous fault identification approach has been proposed by Yan et al. (2021) to identify the source of the faults, whether the faults are caused by sensors or by gas-turbine gas paths. Biddle and Fallah (2021) have introduced an identification approach for faults occurring simultaneously at multiple sensors in autonomous vehicle controllers via multi-class SVM models. Taimoor et al. (2021) have proposed using adaptive radial basis functions for sensor fault identification or quadrotor unmanned aerial vehicles. Aiming to identify sensor faults of gas turbine engines, Zhu et al. (2020) have introduced a residual-based scheme to identify single and simultaneous sensor faults occurring at different sensors.

In this study, an FD methodology for the "identification of combined sensor faults (ICSF)", referred to as "ICSF methodology", is proposed to identify combined sensor faults simultaneously affecting individual sensors. The ICSF methodology builds upon a classification LSTM network and is validated using acceleration measurements from a real-world SHM system installed on a pedestrian bridge. The results of the validation tests prove the capability of the ICSF methodology to identify combined sensor

faults, thus improving the quality of FD by comprehending the causes of sensor faults in real-world SHM systems.

The remainder of the paper is structured as follows. First, the ICSF methodology, tailored to sensors of SHM systems, is introduced. Next, the implementation of the ICSF methodology is illustrated and validated using real-world sensor data (i.e., acceleration measurements). Then, the results are presented and discussed. Finally, the summary of the study and the conclusions are provided, along with potential future work directions.

2. A methodology for identifying combined sensor faults in SHM systems

This section presents the ICSF methodology for SHM systems. First, background information on combined faults is provided. Then, the classification model is presented, which is integrated into the ICSF methodology, described thereafter, for identifying combined sensor faults.

2.1 Combined sensor faults

Sensor faults, depending on the fault types, leave unique traces on sensor data (Dragos and Smarsly, 2016). For example, bias occurs when sensor data exhibits constant divergence from actual sensor data. Drift is represented by progressive deviations of sensor data from actual sensor data with time. Gain is observed when sensor data is scaled by a constant value. Precision degradation manifests when sensor data is contaminated with white noise. Complete failure is represented by replacing sensor data over time either with a constant value ("constant complete failure") or with noise ("noisy complete failure"), regardless of changes occurring in actual structural responses. An outlier is apparent in the form of discontinuous observations that deviate from sensor data at individual time instances (Dervilis et al., 2016).

In real-world SHM systems, faulty sensors may exhibit single sensor faults or combined sensor faults. As an example, the manifestation of a combined sensor fault that consists of drift and an outlier is illustrated in Figure 1. As a result, fault identification must address both fault categories, i.e. single sensor faults and combined sensor faults, requiring sophisticated classification networks, such as LSTM networks, which are used in this paper and briefly described in the following subsection.

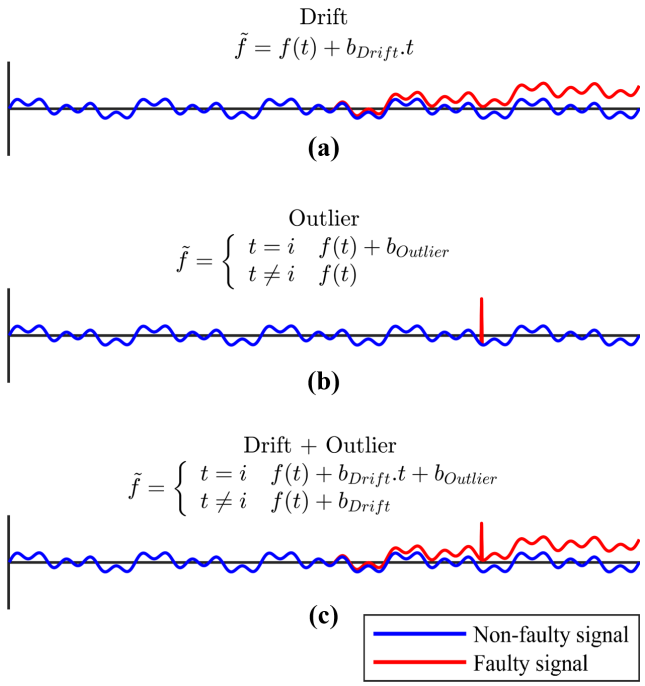

Figure 1: Illustration of a combined sensor fault: (a) A single sensor fault with a drift, (b) a single sensor fault with an outlier, and (c) a combined sensor fault consisting of a drift and an outlier

2.2 Long short-term memory networks for classification

Long short-term memory networks have shown formidable performance in conducting complex classification tasks (Fandango, 2018). LSTM networks are extensions to recurrent neural networks for addressing the *vanishing gradient problem*, capable of mapping relationships between input data (in this case, sensor data) and output data (in this case, classes of single and combined sensor faults). From a layout perspective, a typical LSTM network follows the usual neural-network architecture, consisting of one input layer, one or more hidden layers, and one or more output layers, each consisting of several neurons, as shown in Figure 2. The input-output mapping is achieved by training, which involves fine-tuning the weighted connections between the neurons. Similar to recurrent neural networks, connections between neurons in LSTM networks may deviate from the typical unidirectional propagation of data between neurons of successive layers, followed in feedforward neural networks. The input layer is represented by a “sequence input” layer. The number of sequences is equal to the number of sensors considered for the mapping, and the length of each sequence is equal to the number of data points collected by each sensor.

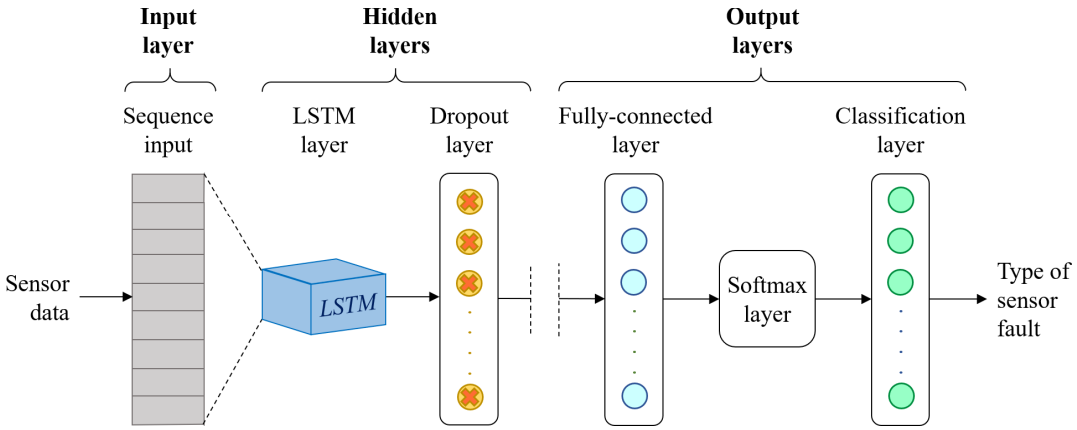

Figure 2: General architecture of the LSTM classification network

The distinct feature of LSTM networks is the architecture of the hidden layers, which consist, as shown on Figure 2, of chains of "LSTM layers" and "dropout layers". A typical LSTM layer, illustrated in Figure 3, comprises four components, a *cell state*, a forget gate, an *input gate*, and an *output gate*. All components accept the input vector $\mathbf{x}_t$ at time t and pass the vector through *activation functions*, i.e. sigmoid functions σ_s for the input, output, and forget gates, and hyperbolic tangent σ_h for the cell, as shown in Equation 1.

$$\begin{aligned}
&\mathbf{y}_{j,t} = \sigma_s\left(\mathbf{W}_j\mathbf{x}_t + \mathbf{U}_j\mathbf{h}_{t-1} + \mathbf{b}_j\right),\ \mathbf{y}_{g,t} = \sigma_s\left(\mathbf{W}_g\mathbf{x}_t + \mathbf{U}_g\mathbf{h}_{t-1} + \mathbf{b}_g\right),\ \mathbf{y}_{o,t} = \sigma_s\left(\mathbf{W}_o\mathbf{x}_t + \mathbf{U}_o\mathbf{h}_{t-1} + \mathbf{b}_o\right) \\
&\hat{\mathbf{c}}_t = \sigma_h\left(\mathbf{W}_{\hat{c}}\mathbf{x}_t + \mathbf{U}_{\hat{c}}\mathbf{h}_{t-1} + \mathbf{b}_{\hat{c}}\right) \\
&\sigma_s(z) = \frac{1}{1+e^{-z}},\ \sigma_h(z) = \frac{e^{2z}-1}{e^{2z}+1}
\end{aligned} \tag{1}$$

In Equation 1, $\mathbf{y}$ represents the outcome of activation functions ("activations"), and the subscripts j, g and o, denote the input gate, the forget gate, and the output gate, respectively. The matrix $\mathbf{W}$ holds the "input" weights, i.e. the weights of connections with neurons of the previous layer, and $\mathbf{U}$ is the matrix of "recurrent" weights, i.e. the weights of connections of the output of the LSTM layer $\mathbf{h}_{t-1}$ at the previous time step to itself. The vector $\mathbf{b}$ is the activation threshold for each component, and $\hat{\mathbf{c}}$ is the outcome of activation of the cell component. In the first LSTM layer, $\mathbf{x}_t$ is the input data vector, and in the next LSTM layers, $\mathbf{x}_t$ is the output of the previous layer.

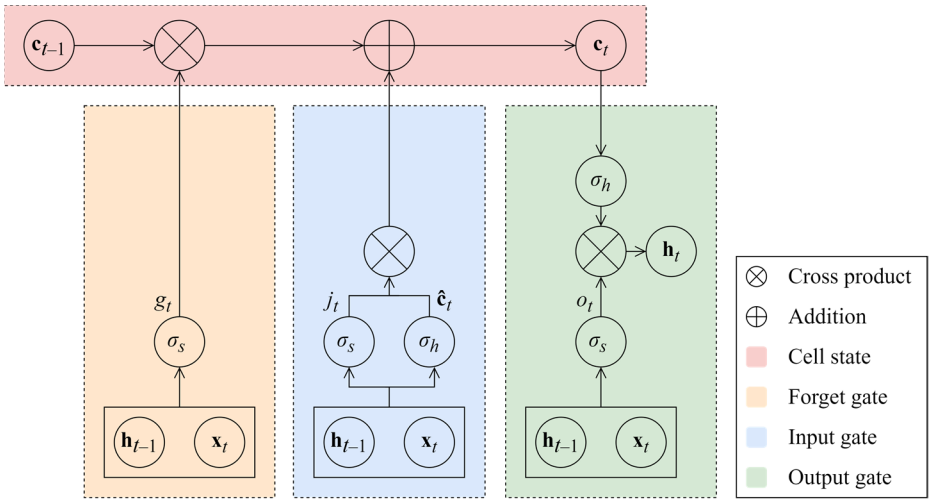

Figure 3: Components of a hidden layer in an LSTM network

The functionality of the LSTM lies in its capability to maintain arbitrary past values in the cell component ("long-term memory", $\mathbf{c}_{t\text{-}1}$) and to use the past values along with values of time t–1 ("short-term memory", $\mathbf{h}_{t\text{-}1}$) to produce the output of the layer at time t ($\mathbf{h}_t$):

$$\mathbf{c}_t = \mathbf{y}_{g,t} \Theta \mathbf{c}_{t-1} + \mathbf{y}_{j,t} \Theta \hat{\mathbf{c}}_t, \mathbf{h}_t = \mathbf{y}_{o,t} \Theta \sigma_h (\mathbf{c}_t), \quad (2)$$

with $\mathbf{c}_0 = \mathbf{h}_0 = \mathbf{0}$. From Equation 2, it follows that, at each time step, the information to be maintained in the cell component as long-term memory is obtained based on the activation of the forget gate, with activation values close to $\sigma_s(z) = 0$ resulting in discarding values from the long-term memory (Fandango, 2018). Each LSTM layer is followed by a dropout layer, which prevents overfitting by defining a "dropout rate", i.e. a fraction of data to randomly be "dropped out" (ignored) during training.

The output layers consist of one "fully-connected layer", one "Softmax" layer, and one "classification layer". The fully-connected layer receives inputs from the last dropout layer and its activations are passed to the classification layer, which contains the classes of single and combined sensor faults to be identified. The Softmax layer is placed between the fully-connected layer and the classification for converting the activations of the fully-connected layer into probability distributions for each class.

The proposed ICSF methodology essentially involves creating and training LSTM networks to develop classification models for identifying both single sensor faults and combined sensor faults. The methodology comprises two activities, each encompassing several actions, as described in the following subsection.

2.3 Description of the ICSF methodology

The ICSF methodology is illustrated in Figure 4 in terms of an activity diagram, comprising two activities, (1) "preparing the training dataset" and (2) "developing the classification models". The first activity is composed of four actions, and the second activity encompasses three actions.

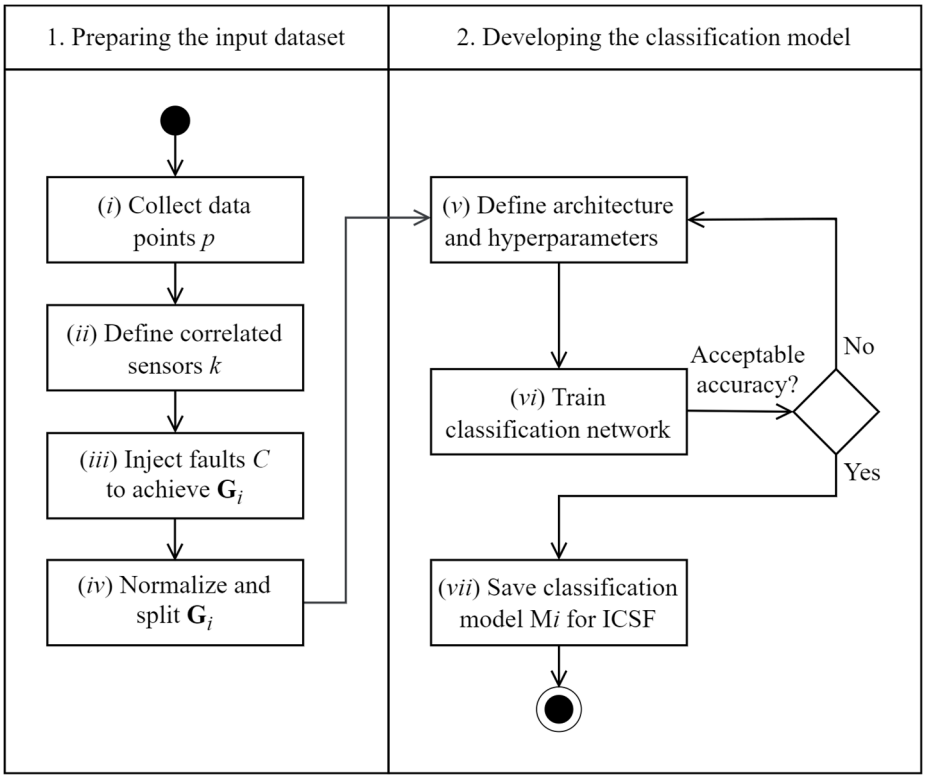

Figure 4: Activities and actions within the ICSF methodology

Within the first activity, *action* (*i*) involves collecting data by the sensors of the SHM system in the "data collection period", where p is the number of data points collected by each sensor. In *action* (*ii*), correlation analysis is conducted on the sensor data to define the number of correlated sensors k in the SHM system, which corresponds to the number of sequences in the LSTM input layer. Each sensor within the set of correlated sensors is labeled as i ($i = 1, \ldots, k$). Then, data collected by correlated sensors $\mathbf{f}_{1\to k}$ is stored in a matrix $\mathbf{A}^{p\times k}$, as shown in Equation 3 below:

$$\mathbf{A}^{p\times k} = \begin{bmatrix} \mathbf{f}_1 & \mathbf{f}_2 & \cdots & \mathbf{f}_k \end{bmatrix} = \begin{bmatrix} f_{1,1} & f_{1,2} & \cdots & f_{1,k} \\ f_{2,1} & f_{2,2} & \cdots & f_{2,k} \\ \vdots & \vdots & \ddots & \vdots \\ f_{p,1} & f_{p,2} & \cdots & f_{p,k} \end{bmatrix} \tag{3}$$

In *action* (*iii*), sensor faults are artificially injected into the sensor data. The reason for injecting faults is to train the classification networks for identifying real-world combined sensor faults. The sensor data

stored in matrix **A** is duplicated into the input dataset $\mathbf{G}_i$ (i = 1, …, k). Both single and combined sensor faults are then artificially injected into the vector $\mathbf{f}_i$, which indicates the sensor data collected by sensor i. The types of injected sensor faults are stored in the corresponding classification output dataset $\mathbf{O}_i$. Consequently, the input dataset $\mathbf{G}_i$ comprises non-faulty data from sensors (1, 2, …, i-1, …, k), along with sensor data from sensor i featuring single and combined sensor faults.

As shown in Equation 4, the total number of sensor fault types C injected into the dataset depends on the number of single fault types N, the number of single fault types n included in the combinations, and the number of single fault types m included in each combination:

$$C(n,m) = \frac{n!}{m!(n-m)!} + N \tag{4}$$

In *action* (*iv*), the sensor data in the input dataset $\mathbf{G}_i$ is normalized using a minimum-maximum normalization method, as shown in Equation 5. The rationale behind data normalization is to avoid overfitting in the classification models by preventing extreme values in the data, which could otherwise impede the training process by causing numerical instability or convergence issues. In Equation 5, $x_{normalized}$ represents the normalized values, x represents a measurement in the sensor data, and the normalization parameters $x_{\min}$ and $x_{\max}$ represent the minimum and maximum measurements in the sensor data, respectively. The normalization parameters $x_{\min}$ and $x_{\max}$ used for $\mathbf{G}_i$ are saved for future use on sensor data fed into the classification model M_i, which is the LSTM-based model that is able to identify single and combined sensor faults occurring in sensor i.

$$x_{normalized} = \frac{x - x_{\min}}{x_{\max} - x_{\min}} \tag{5}$$

Thereafter, the normalized input dataset $\tilde{\mathbf{G}}_{\underline{i}}$ is split into training dataset $\mathbf{G}_{t,i}$, validation dataset $\mathbf{G}_{v,i}$, and testing dataset $\mathbf{G}_{s,i}$. The datasets are labeled and used for training the classification networks to develop the classification models.

Within the second activity, *action* (*v*) defines an initial architecture and the hyperparameters of the LSTM classification network. The hyperparameters include the layers comprising the network, the activation functions, the optimizer, the number of epochs, and the batch size.

Action (*vi*) involves training the classification networks with the training dataset $\mathbf{G}_{t,i}$ to create the classification model M_i for each correlated sensor i (i = 1, …, k). Throughout training, the training

dataset $\mathbf{G}_{t,i}$ is sequentially fed to the input layer of the LSTM classification network in batches. The corresponding classes of the output dataset $\mathbf{O}_{t,i}$ are fed into the output layer. The propagation of a single batch through the LSTM classification network is a training "iteration", and, as soon as all batches have been passed through the network, one "epoch" is completed. Training involves adjusting the weighted connections between neurons in each iteration until the probabilities at the Softmax layer achieve a predetermined level of accuracy. The resulting classification model M_i is able to recognize features in the input dataset $\tilde{\mathbf{G}}_i$ and classify the sensor data into the corresponding combined sensor fault types. During training, in predefined intervals (e.g. after a predefined number of iterations), the validation dataset $\mathbf{G}_{v,i}$ is passed through the LSTM classification network to confirm the prediction accuracy trend with an independent set of sensor data and, thus, avoid overfitting to the training dataset and, furthermore, to fine-tune the hyperparameters so as to improve training.

Upon completing training, the accuracy of each classification model is checked using the testing dataset $\mathbf{G}_{s,i}$. The accuracy (a) of the classification model M_i is calculated by measuring the number of correct predictions – true positives (TP) and true negatives (TN) – among the total number of predictions (NP), according to Equation 6.

$$a = \frac{\mathrm{TP} + \mathrm{TN}}{\mathrm{NP}} \tag{6}$$

The accuracy essentially measures the "correctness" of the classification model as a whole. To evaluate the classification performance of the model, the "precision" and "recall" metrics are used. Precision (pr) and recall (rc) indicate the capabilities of the model to avoid false positive classifications and false negative classifications, respectively, as shown in Equation 7.

$$pr = \frac{\mathrm{TP}}{\mathrm{TP} + \mathrm{FP}} \qquad rc = \frac{\mathrm{TP}}{\mathrm{TP} + \mathrm{FN}}, \tag{7}$$

where FP is the number of false positives, and FN is the number of false negatives. If the accuracy of the classification model M_i is satisfactory, the model is saved in *action* (*vii*) to be used for ICSF of sensor *i*. However, an unsatisfactory accuracy of the model requires defining a different architecture of the LSTM classification network and training a new classification network, reverting to the fifth action. The same process is repeated for all sensors. The implementation of the ICSF methodology is illustrated in the following section.

3. Implementation and Validation of the ICSF methodology

In this section, the implementation and validation of the ICSF methodology are detailed. The description of the ICSF methodology implementation is structured according to the activities of the ICSF methodology presented in the previous section, i.e. "preparation of the training dataset" and "development of the classification models". The validation tests are then performed to show the capability of the ICSF methodology of identifying combined sensor faults of real-world SHM systems. Both validation tests are carried out using sensor data (i.e., acceleration measurements) from an SHM system operating on a pedestrian overpass bridge located in Evosmos, Thessaloniki, Greece. The *first validation test* involves sensor faults that are artificially injected into non-faulty acceleration measurements collected by the SHM system. In the *second validation test*, a faulty accelerometer is placed within close proximity of a non-faulty accelerometer of the SHM system, i.e. real sensor faults instead of artificially injected sensor faults are considered to validate the ICSF methodology. In what follows, the ICSF methodology implementation is illustrated. Then, the pedestrian bridge and the SHM system used in the validation tests are described, followed by the presentation of the validation tests and the discussion of the results.

3.1. Implementation of the ICSF methodology

The implementation of the two activities of the ICSF methodology is shown in this subsection. An in-depth explanation of how both fault categories (single and combined) are generated and injected into the sensor data for training purposes is provided, followed by a description of the development of the classification models, based on LSTM networks.

For implementing the ICSF methodology, a SHM system installed on a structure with sensors and a data acquisition unit for transferring the sensor data to a centralized server, where the data is stored and analyzed, is deployed. The sensor data is used for preparing the training data set. To enhance the training accuracy, care is taken that the sensor data, collected in the data-collection period, is representative of the structural conditions and loading scenarios anticipated under normal operation. Data analysis is conducted via "functions", written using MATLAB (MathWorks, Natick, MA, 2022). First, Pearson correlation analysis is conducted to define the number of correlated sensors k and to create matrix $\mathbf{A}_{p \times k}$. Next, sensor faults are calculated and injected into matrix $\mathbf{A}$ and for creating the input dataset $\mathbf{G}_i$ (i = 1, …, k). Labels of sensor faults, generated and injected, are stored in the classification output dataset $\mathbf{O}_i$ (i = 1, …, k). Then, minimum-maximum normalization is performed, as shown in Equation 5. Both normalization parameters, $x_{\min}$ and $x_{\max}$, for the input dataset i, are saved and used to normalize newly collected sensor data that is fed to the classification model M_i after training. Finally, the normalized dataset $\tilde{\mathbf{G}}_i$ is split into training data (70 %), validation data (15 %), and testing data (15 %).

After preparing the training data, the classification models are developed. The process of sensor fault identification, through the development of classification models, is introduced herein. The ICSF methodology represents an extension of preliminary work, conducted by the authors (Al-Zuriqat et al., 2023), in which insights pertaining to sensor fault detection, isolation, and accommodation are provided.

To develop the classification models, an initial architecture of the classification networks, with a total number of networks equal to the number of the correlated sensors k, is defined based on the general architecture of LSTM networks, shown in Figure 2. The input layer is defined along with an initial number of hidden LSTM layers and dropout layers with a dropout rate of 0.2 to avoid overfitting. The fully connected layer is then defined, followed by the Softmax layer for the classification task and the classification output layer. The classification networks with the initial architecture are trained, in which the networks utilize pre-existing associations between established input data (data collected by correlated sensors with injected faults), and corresponding output data (injected fault type). Then, the other hyperparameters are defined, including the optimizer, the number of epochs, and the batch size. Thereafter, the accuracy of the trained models is evaluated using the testing data set, as illustrated in Equation 6, based on the previously derived threshold γ. Until the accuracy of the models is satisfactory, the architecture and hyperparameters of the networks are modified and the networks are retained. Finally, the classification models, which demonstrate satisfactory accuracy when evaluated with the testing data, are saved for identifying combined sensor faults using new sensor data.

After the implementation, validation is conducted essential for proving that capability of identifying combined sensor faults. The ICSF methodology is validated using the real-world SHM system installed on the pedestrian bridge, as further illuminated.

3.2. Description of the pedestrian bridge and the SHM system

The pedestrian overpass bridge, shown in Figure 5, serves pedestrian traffic over the Inner Ring Road of Thessaloniki, and it has been a subject of research in previous studies (Dragos et al., 2020; Smarsly et al., 2022a; and Smarsly et al., 2022b). Constructed in 2016, the pedestrian bridge consists of a composite structure, where a steel structure supports a reinforced-concrete deck. The composite structure rests on two steel girders at both ends with square hollow sections. The dimensions of the reinforced-concrete deck are 35.00 m in length and 4.60 m in width. Cylindrical reinforced-concrete columns support the girders at each end of the composite structure, and the connections between the girders and the columns are realized using elastomeric bearings that allow partial fixity. To ensure load transfer, the composite structure features two inwardly inclined steel arches. The arches have square hollow cross-sections, are connected to the composite structure by steel cables, and are fully welded to

the girders at the ends. The lateral stability of the bridge is enhanced through steel beams connecting the main girders at equidistant points.

Figure 5: The pedestrian bridge in Evosmos, Thessaloniki, Greece

The SHM system comprises four accelerometers, S_1, S_2, S_3, and S_4, which have been previously tested and found to be non-faulty. The accelerometers are equally distributed along the central axis spanning the length of the bridge, spaced 7 m apart from each other, ignoring both ends of the bridge above the supporting columns, at which accelerations have negligible impact on the structural behavior of the bridge. In addition to the four non-faulty accelerometers, a "faulty" accelerometer, denoted by FS_2, proven to be faulty in previous experiments, is placed within a close proximity to the non-faulty accelerometer S_2. Figure 6 presents the top view of the pedestrian bridge and the locations of the faulty and non-faulty accelerometers used in the validation tests.

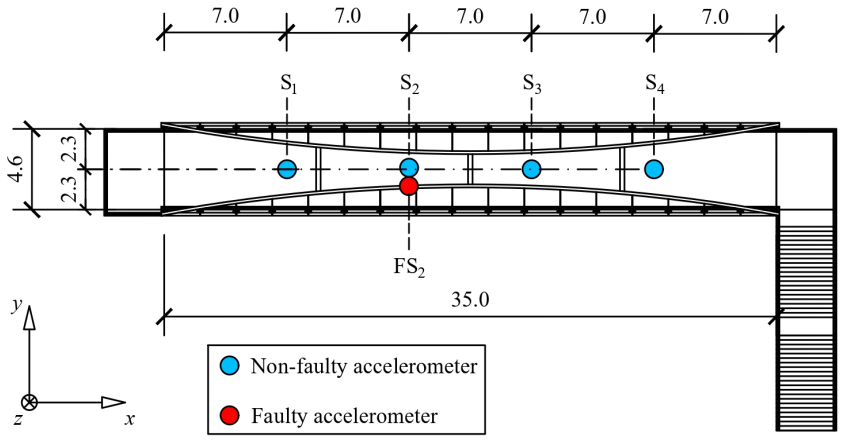

Figure 6: Top view of the pedestrian overpass bridge with the locations of the accelerometers

3.3. Description of the validation tests

First validation test (artificially injected sensor faults)

In the *first validation test*, acceleration measurements are collected by the four accelerometers, S_1, S_2, S_3 and S_4, over a 90-minute data collection period at a sampling rate of 128 Hz, as part of the first activity of the ICSF methodology. Each accelerometer collects a total of p = 692,628 data points. Next, the correlated sensors are defined through correlation analysis on the acceleration measurements. The Pearson correlation coefficient reveals a strong correlation (> 0.90) among all four accelerometers, i.e. k = 4. The lowest correlation coefficient observed is 0.937, between sensors S_1 and S_4. Following the correlation analysis, the acceleration measurements from all four correlated accelerometers $f_{1\rightarrow k=4}$, are stored in matrix $\mathbf{A}_{692628\times4}$.

Seven single faults (N = 7) are considered, comprising bias, drift, gain, precision degradation, complete failure (constant and noisy), and outliers. Concerning combined sensor faults, combinations of two single faults within the same sensor (m = 2) are considered. For instance, a combination may involve simultaneous occurrence of drift and outlier within an individual sensor. Complete failure, both constant and noisy, involves sensors stopping operation and, thus, cannot be combined with other single faults; therefore, complete failures are excluded from combinations (n = 5). The total number of sensor fault types is C (n, m) = 17, computed with Equation 4. Table 1 shows an overview of the sensor fault types of both categories, single and combined, considered in the validation tests. Furthermore, visual representations of the single and combined sensor fault types are given in Figures 7 and 8.

Table 1: Sensor fault types considered in the validation tests

Fault category	Sensor fault type	Description	Class No.
Single faults	Bias	Included in the combinations	1
	Drift		2
	Gain		3
	Precision degradation		4
	Outlier		5
	Complete failure (constant)	Excluded from the combinations	6
	Complete failure (noisy)		7
Composite faults	Bias + Drift		8
	Bias + Gain		9
	Bias + Precision degradation		10
	Bias + Outliers		11

Drift + Gain	12
Drift + Precision degradation	13
Drift + Outliers	14
Gain + Precision degradation	15
Gain + Outliers	16
Precision degradation + Outliers	17

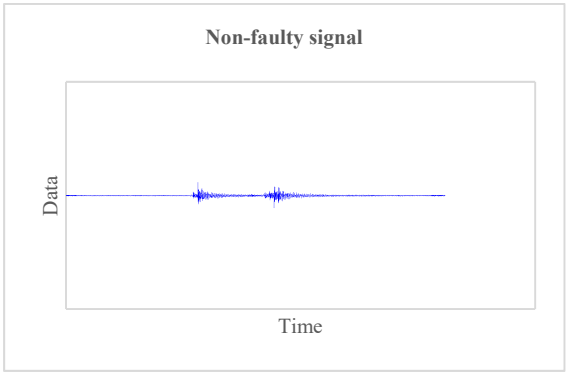

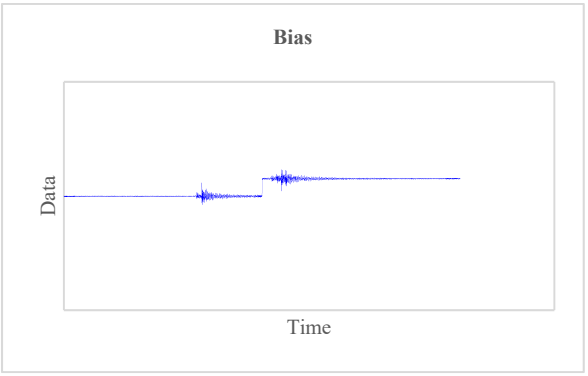

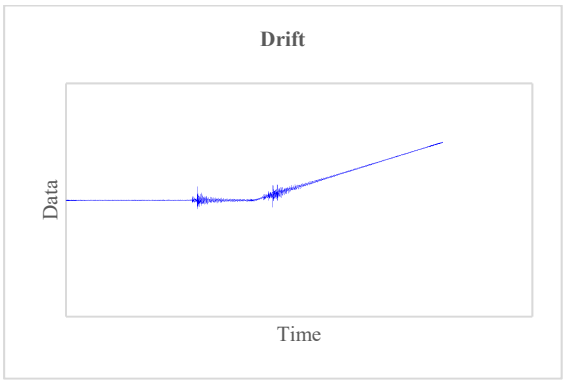

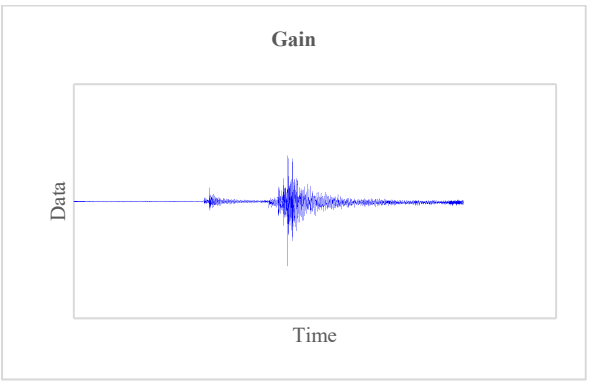

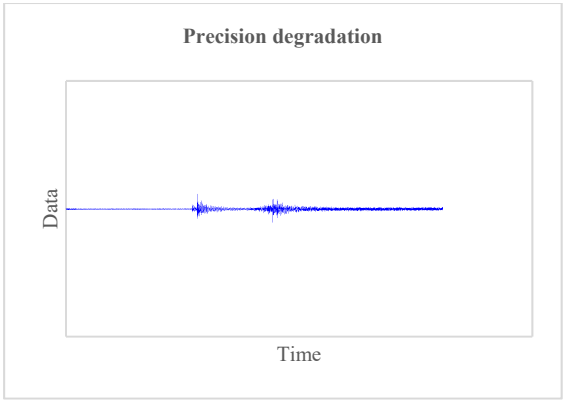

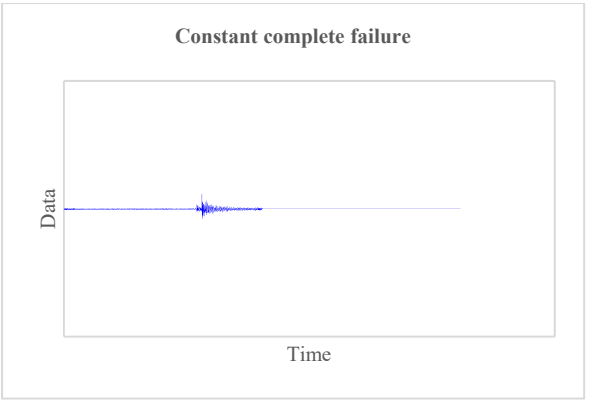

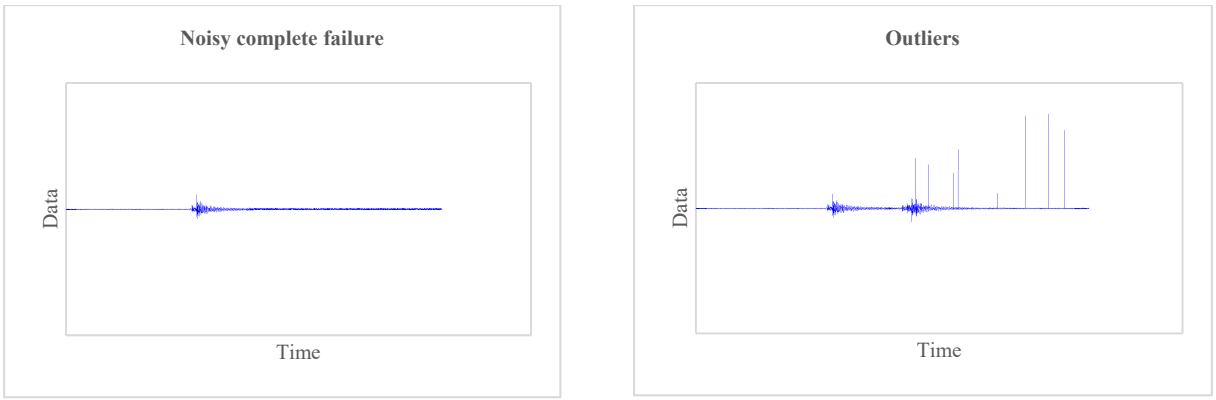

Figure 7: Qualitative representation of single sensor fault types included in the validation tests

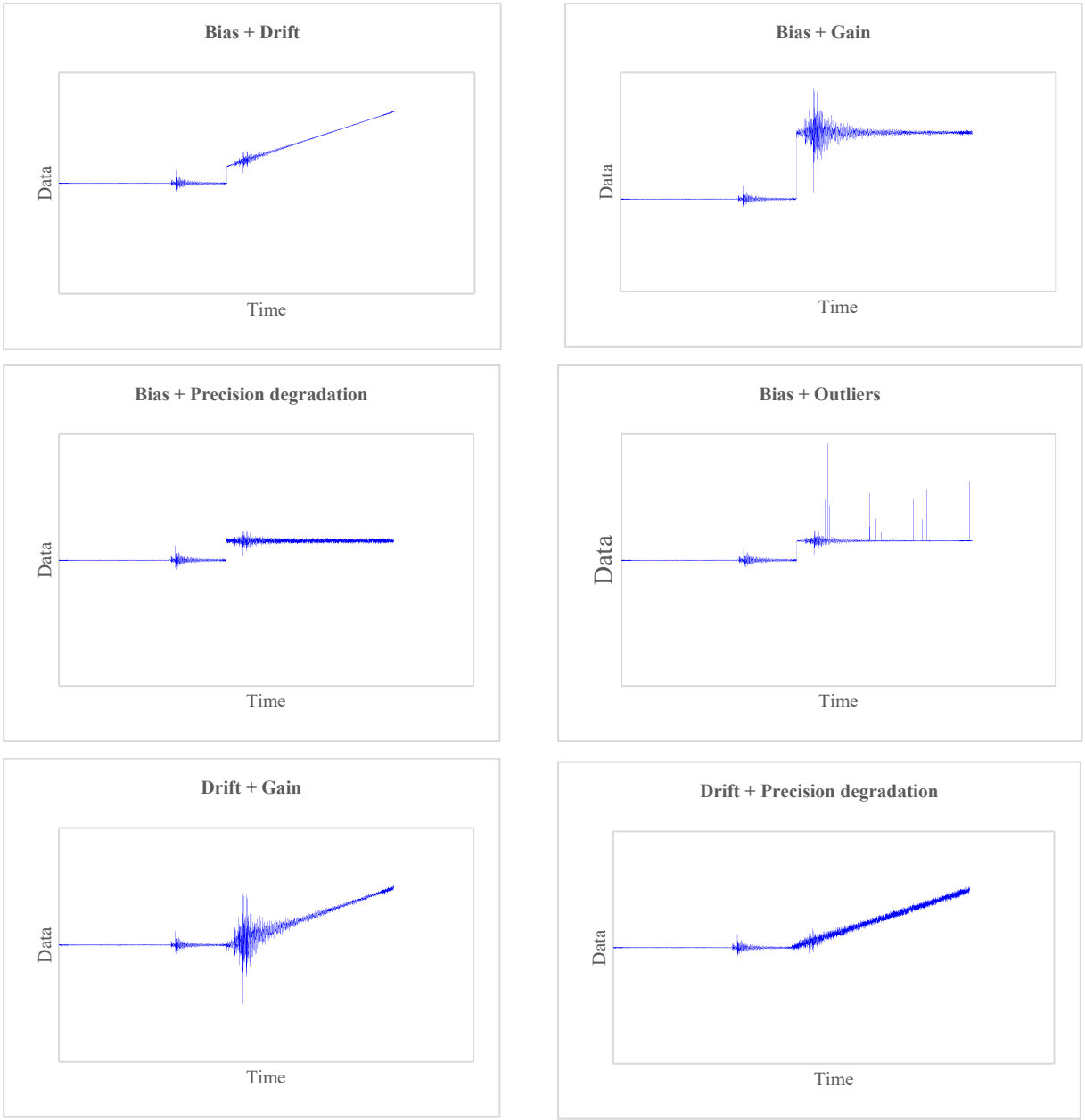

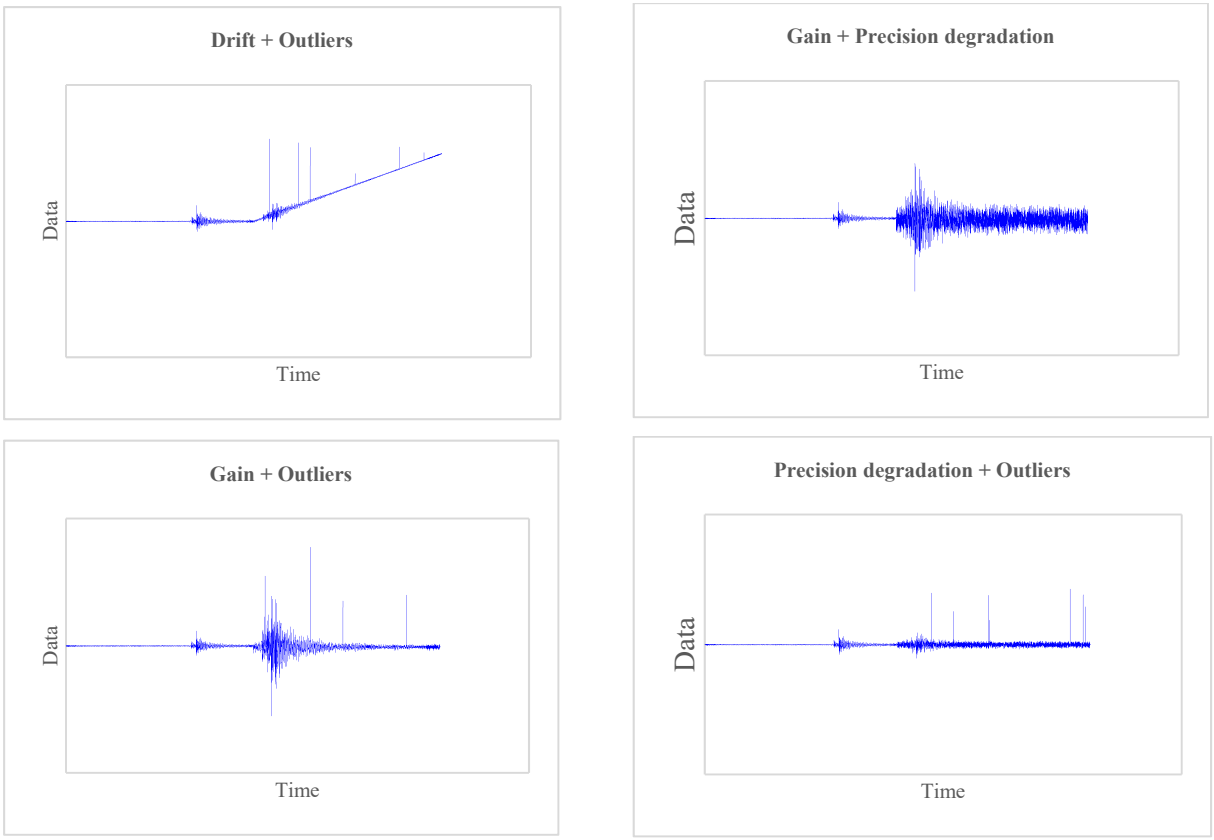

Figure 8: Qualitative representation of combined sensor fault types included in the validation tests

The acceleration measurements, previously stored in matrix $\mathbf{A}_{692628\times4}$, are used to create the four input datasets, each evenly divided into 17 subsets, where each of the sensor fault types, shown in Table 1, is artificially injected. The classes of the sensor fault types injected into the input dataset $\mathbf{G}_i$ (i = 1, …, 4) are stored in the corresponding output dataset $\mathbf{O}_i$ (i = 1, …, 4). Thereafter, the acceleration measurements of the input dataset i are normalized, according to Equation 5, and the normalized input dataset $\tilde{\mathbf{G}}_i$ is divided into 70 % training dataset (484,838 data points), 15 % validation dataset (103,894 data points), and 15 % testing data (103,894 data points). The normalization parameters, $x_{\min}$ and $x_{\max}$, employed for the input dataset i during training are saved for application to new sensor data fed into the classification model M_i.

The initial architecture for the LSTM classification network is defined, featuring a sequence input layer with length equal to the number of correlated sensors k = 4. The output layer comprises a fully-connected layer, the Softmax layer, and a classification layer with 17 classes, representing one sensor fault per class, as shown in Table 1. After a trial-and-error process, three hidden layers are defined, each layer is composed of an LSTM layer followed by a dropout layer, with the probabilities of the dropout layers uniformly set to 20 %. Four classification models, corresponding to the number of the correlated sensors (k = 4), are developed. The network architectures of all four models are chosen to be the same. Each model M_i classifies sensor fault types of sensor i, using acceleration measurements from the four correlated sensors of the SHM system as input data. Figure 9 illustrates the network architecture of the

classification models M_1, M_2, M_3, and M_4, each dedicated to classifying the sensor fault types in sensors S_1, S_2, S_3, and S_4, respectively. It should be noted that the total training time for each classification models M_1, M_2, M_3, and M_4 are recorded as 62 minutes, 69 minutes, 56 minutes, and 128 minutes, respectively, trained on a computer equipped with a GPU, boasting 10GB of GDDR6X memory, and operating at a speed of 1188 MHz.

Based on Equation 6, the accuracy of the models is assessed with the testing dataset comprising 103,894 data points. The level-of-accuracy threshold is set to 85 %, based on previous experience from fault detection (Al-Zuriqat et al., 2023). Upon completing training, it is observed that the model M_2 exhibits the lowest accuracy of 90.3 %. The results are discussed in the next section, together with the results of the second validation test.

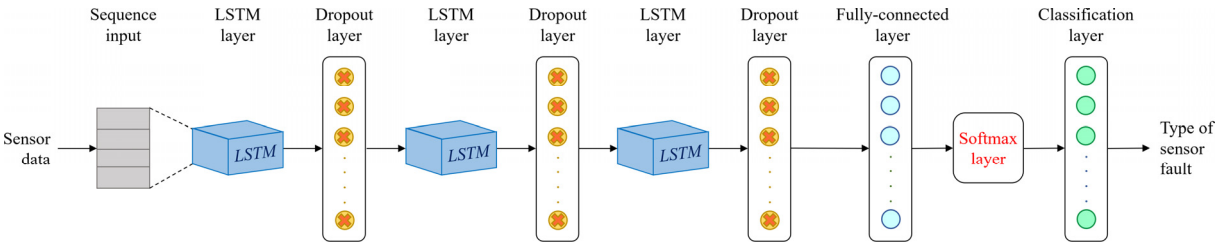

Figure 9: Network architecture of the classification models M_1, M_2, M_3, and M_4 used in the validation tests

Second validation test (real-world sensor faults)

The *second validation test* covers sensor faults obtained from the real-world SHM system using the faulty accelerometer FS_2. The classification model M_2, previously trained to identify faults for the non-faulty sensor S_2, is used to identify sensor faults for the faulty accelerometer FS_2. Specifically, data collected by S_1, FS2, S_3, and S_4 is used as input for the classification model M_2.

Unlike the first validation test, where sensor faults are artificially injected under controlled conditions, no prior knowledge is available about the locations of the sensor faults existing in the dataset of FS_2 or about the types of the sensor faults. The acceleration measurements used in this validation test correspond to a data collection period of approximately 7 minutes at a sampling rate of 128 Hz. In the data collection period, the total number of data points collected by each of the accelerometers, i.e. S_1, FS_2, S_3, S_4, and FS_2, is p = 53,688 data points. To validate the fault identification capability of the classification model M_2, the acceleration measurements collected by the faulty accelerometer FS_2 are visualized and compared with the acceleration measurements collected by the non-faulty sensor S_2, as shown in Figure 10.

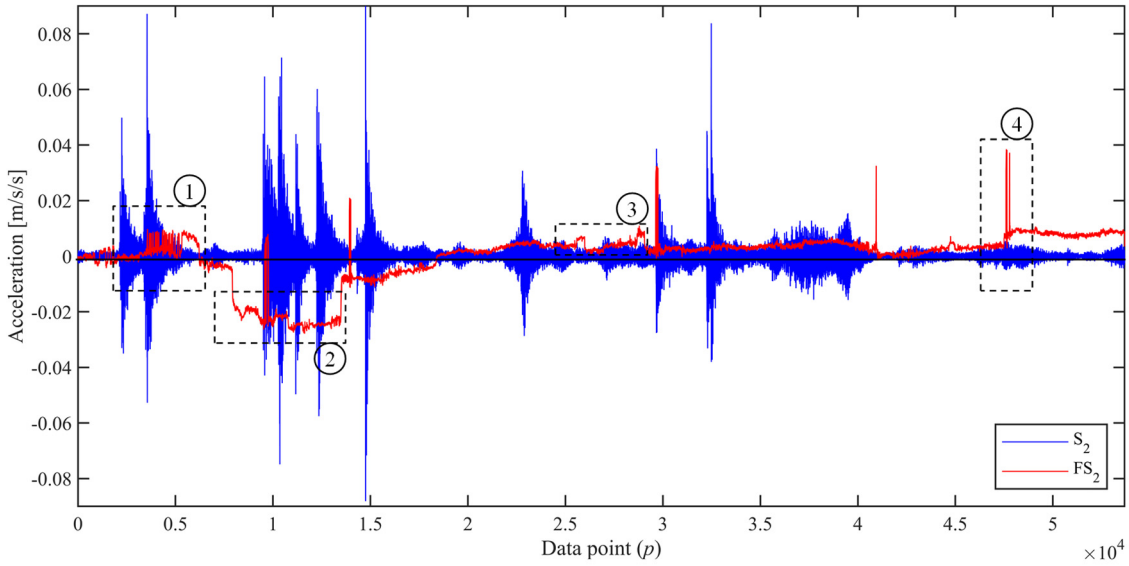

Figure 10: Time-history of acceleration measurements collected by the non-faulty sensor S_2 *and the faulty sensor* FS_2

As depicted in Figure 10, the acceleration measurements collected by the faulty accelerometer FS_2 exhibit a noticeable deviation from the data captured by the accelerometer S_2 due to the faults featured in FS_2. To focus on the main goal of identifying combined sensor faults, a detailed analysis is conducted on data within windows 1, 2, 3, and 4, marked in Figure 10. The results of the validation tests are presented and discussed in the next section.

4. Results and discussion

This section presents the results of both validation tests. The results are first tabulated, followed by a discussion on the capability of the ICSF methodology to identify combined sensor faults in SHM systems.

4.1. Identification of artificially injected sensor faults

This subsection showcases the results of applying the classification models, M_1, M_2, M_3 and M_4, obtained via the ICSF methodology, on newly collected acceleration measurements artificially injected with sensor faults. Table 2 shows the fault identification results of all the classification models using the newly collected acceleration measurements with artificially injected sensor faults. The results include accuracy values, as well as precision and recall metrics for each sensor fault and each classification model. As noted from Table 2, the lowest precision value of 62.5 % is achieved by model M_1, predicting the single sensor fault type “Outlier”. Moreover, the lowest recall values of 11.7 %, 4.8 %, 8.5 %, and 57.2 % are achieved by the four models M_1, M_2, M_3, and M_4, respectively, from predicting the same combined sensor fault type “Drift + Outliers”.

Table 2: ICSF results of the precision (pr), recall (rc), and accuracy (a) of the artificially injected sensor faults

Fault category	Sensor fault type	No.	M_1		M_2		M_3		M_4	
			pr (%)	*rc* (%)	*pr* (%)	*rc* (%)	*pr* (%)	*rc* (%)	*pr* (%)	*rc* (%)
Single faults	Bias	1	98.1	94.4	95.4	97.7	96.6	97.9	96.9	97.3
	Drift	2	78.6	98.3	79.0	97.2	81.0	97.9	88.8	92.5
	Gain	3	98.7	99.3	96.6	97.2	95.1	98.3	98.6	97.9
	Precision degradation	4	94.6	97.8	92.7	95.0	95.6	97.4	90.2	76.8
	Outlier	5	62.5	82.0	89.3	91.6	91.8	87.6	66.3	75.2
	Complete failure (constant)	6	99.1	99.4	99.8	99.9	99.2	99.6	99.9	99.8
	Complete failure (noisy)	7	98.0	99.5	99.8	99.8	99.6	99.1	99.7	99.7
Composite faults	Bias + Drift	8	98.9	96.5	89.8	89.9	93.7	93.1	98.0	99.9
	Bias + Gain	9	97.6	99.2	99.5	100.0	97.0	99.0	99.5	99.8
	Bias + Precision degradation	10	99.9	98.0	95.2	99.4	99.9	98.4	77.2	95.8
	Bias + Outliers	11	72.9	66.7	99.5	85.0	92.8	87.4	95.8	90.3
	Drift + Gain	12	97.8	91.7	78.6	61.1	88.2	91.8	88.4	94.4
	Drift + Precision degradation	13	99.4	96.7	70.6	82.2	95.9	90.6	99.8	93.2
	Drift + Outliers	14	95.6	11.7	69.4	4.8	83.3	8.5	73.5	57.2
	Gain + Precision degradation	15	97.1	98.6	94.9	96.3	98.6	98.0	98.3	99.9
	Gain + Outliers	16	97.1	94.5	87.3	84.8	92.2	92.1	96.0	87.7
	Precision degradation + Outliers	17	89.6	76.7	83.1	78.2	85.2	80.1	69.5	64.9
Accuracy *a*			**93.7 %**		**90.5 %**		**93.8 %**		**92.5 %**	

The accuracy of correctly identifying sensor faults for models M_1, M_2, M_3, and M_4 stands at 93.7 %, 90.5 %, 93.8 %, and 92.5 %, respectively, concluding that all models are capable of achieving acceptably accurate classification. Details on identifying single and combined sensor faults for model M_3 are exemplarily illustrated in Figure 11, in the form of a confusion matrix. The confusion matrix shows the precision and recall values of all classes included in both categories of single and combined sensor faults, following the same numbering as in Table 1. The precision values are depicted at the bottom of the confusion matrix, and the recall values are shown at the right of the confusion matrix, based on Equation 7.

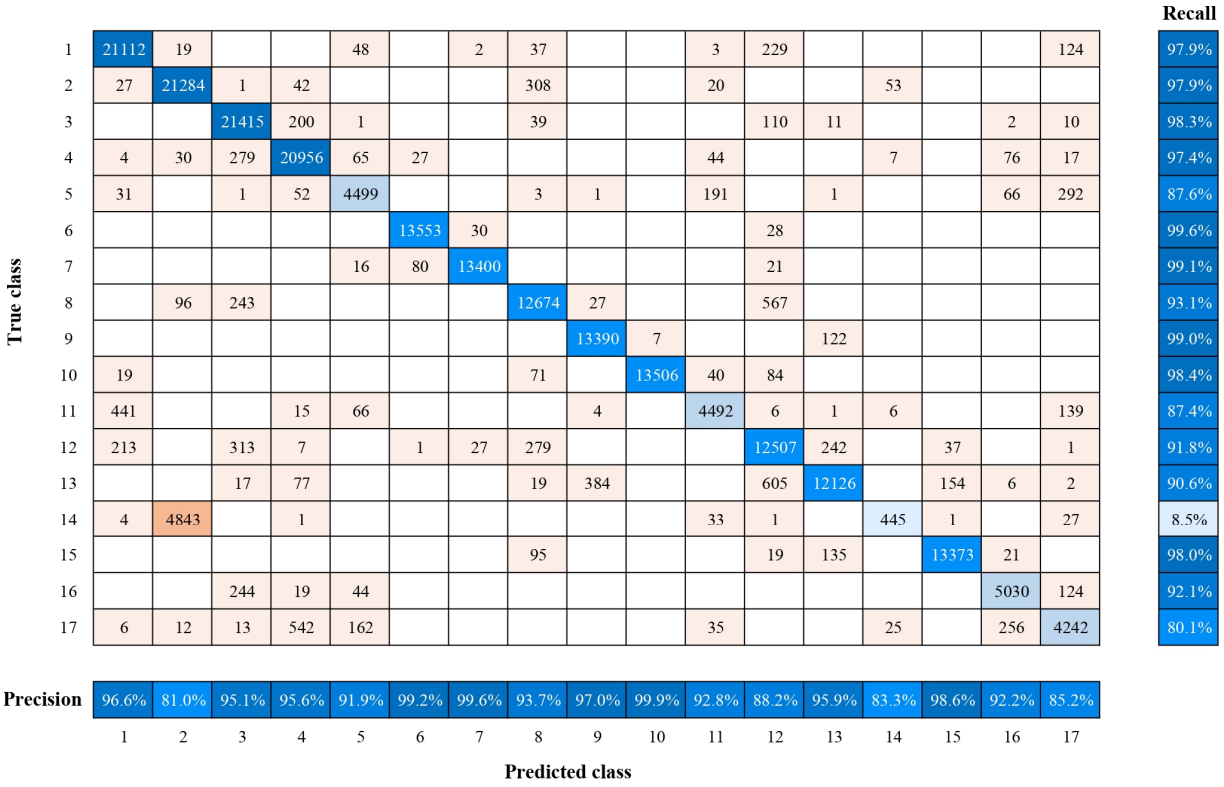

Figure (11): Confusion matrix of all sensor fault types injected into sensor S_3

As noted from Figure 11, the precision values among all 17 classes range between 81.0 % and 99.9 %. Furthermore, the recall values range between 80.1 % and 99.6 %, except for class 14, referring to the combined sensor fault type "Drift + Outliers" with a recall value of 8.5 %. The reason of facing difficulties identifying outliers arises from the subtle patterns that outliers exhibit, characterized by intermittent observations occurring at isolated time points within a continuous signal, causing imbalanced training data.

4.2 Identification of real-world sensor faults

The results of applying the ICSF methodology with acceleration measurements newly collected by the faulty accelerometer FS_2 in the second validation test are presented herein. Table 3 shows the number of sensor faults correctly identified by the ICSF methodology in the acceleration measurements collected by the faulty accelerometer FS_2.

Table 3: Real-world sensor faults identified by the ICSF methodology using data from the faulty-sensor FS_2

Single fault							**Combined faults**									**Total**
Bias	Drift	Gain	Precision degradation	Outlier	Complete failure (constant)	Complete failure (noisy)	Bias + Drift	Bias + Gain	Bias + Precision degradation	Bias + Outliers	Drift + Gain	Drift + Precision degradation	Drift + Outliers	Gain + Precision degradation	Gain + Outliers	Precision degradation + Outliers	
563	32320	11	747	0	1	4248	233	3025	9	0	1762	0	0	0	0	0	42,919

As presented in Table 3, the ICSF methodology has correctly identified a total of 42,919 sensor faults within the acceleration measurements collected by the faulty sensor FS_2. Notably, the most common sensor fault type, constituting nearly 75 % of the total identifications, is a drift. To ensure that the proposed ICSF methodology has correctly identified real-world sensor faults, and since both the faulty accelerometer FS_2 and the non-faulty accelerometer S_2 have been positioned at the same location, the acceleration measurements from both accelerometers are visualized side-by-side, as depicted in Figure 10.

The first window in Figure 10 illustrates the combined sensor fault “Drift + Gain”. The second window starts with downward bias, which is subsequently combined with drift, representing the combined sensor fault “Bias + Drift”. The third window starts with a drift, combined from some point on with a bias to produce the same combined sensor fault “Bias + Drift”. Finally, the fourth window displays the combined sensor fault “Bias + Outliers”. The LSTM classification models have successfully identified the combined sensor faults depicted in windows 1, 2, and 3. However, the combined sensor fault in the fourth window, “Bias + Outliers”, has not been successfully identified by the models. The reason for facing difficulties identifying outliers is the subtle patterns of outliers, which represent intermittent observations at isolated time points within a continuous signal. The subtle patterns of outliers cause imbalanced training data with a smaller number of datasets exhibiting the “outliers” fault compared to the numbers of the datasets exhibiting each of the other faults.

The results shown in both validation tests comprising identification of artificially injected as well as real-world combined sensor faults lead to the conclusion that the ICSF methodology is capable of successfully identifying single sensor faults as well as combined sensor faults. However, the sensor faults “outliers”, whether single or combined with other sensor faults is characterized by low values of precision and recall. Identifying outliers may be difficult for the classification models due to the subtle

patterns of outliers, corresponding to discontinuous observations at isolated time instances in a continuous signal, causing imbalanced training data. Nevertheless, identifying outliers is not critical for FD since outliers may be identified and eliminated from the original signals through signal pre-processing.

5. Summary and conclusions

Fault diagnosis in SHM systems includes fault detection, isolation, identification, and accommodation. Fault identification, so far, has received scarce attention, and FD methods that involved fault identification consider only single sensor faults in individual sensors. Nonetheless, combined sensor faults affecting individual sensors reflect real-world situations, showcasing the importance of ICSF for SHM systems. To improve the quality of FD and to comprehend the causes of sensor faults, this paper has proposed an ICSF methodology. The ICSF methodology is capable of identifying combined sensor faults occurring simultaneously at the same sensor. To address combined sensor faults, sensor data with artificially injected sensor faults has been used to train LSTM classification networks. Sensor data with artificially injected sensor faults has been labeled to enable the classification network to learn the types of faults considered in the ICSF methodology.

To validate the ICSF methodology, two validation tests have been conducted using acceleration measurements from a real-world SHM system installed on a pedestrian bridge, located in Greece. In the first validation test, sensor faults have been artificially injected into acceleration measurements collected by the SHM system. In the second validation test, an accelerometer, which has proven to be faulty based on previous experiments, has been placed within a close proximity to a non-faulty accelerometer of the SHM system. The results of the validation tests have shown that the classification models of the ICSF methodology are capable of identifying combined sensor faults, as exemplarily proven by the fault types bias, drift, gain, precision degradation, and outliers. Nonetheless, due to the imbalanced training data caused by the subtle patterns of outliers, corresponding to discontinuous observations at isolated time instances in a continuous signal, identifying outliers has been challenging for the classification models. However, since outliers can be identified and removed from the original signal through signal pre-processing, the significance of identifying outliers diminishes in FD. In conclusion, the ICSF methodology proposed in this paper has proven the capability to identify combined sensor faults occurring simultaneously at individual sensors, perceiving the causes of sensor faults, representing a step forward to improve FD in SHM systems.

Future research may consider decentralizing the ICSF methodology by embedding the classification models into the sensor nodes of wireless SHM systems, in addition to expanding the methodology to be able to differentiate between sensor faults and structural damage. Moreover, coupling imbalanced-data-

handling methods with the ICSF methodology may be investigated to overcome the imbalanced distribution of training data. Furthermore, the ICSF methodology may be reformulated as a mathematical classification problem to be ready to be complemented with an explanation interface using explainable artificial intelligence, adding transparency to the ICSF methodology.

Acknowledgments

The authors gratefully acknowledge the support offered by the German Research Foundation (DFG) under grants SM 281/17-1 and SM 281/20-1 as well as by the German Federal Ministry for Digital and Transport (BMDV) within the mFUND program under grant 19FS2013B. The financial support is gratefully acknowledged. Any opinions, findings, conclusions, or recommendations expressed in this paper are those of the authors and do not necessarily reflect the views of DFG or BMDV.

Bibliography

Abboush, M., Knieke, C., and Rausch, A. (2023). Intelligent identification of simultaneous faults of automotive software systems under noisy and imbalanced data using ensemble LSTM and random forest. IEEE Access, 11(2023), pp. 140022-140040.

Al-Zuriqat, T., Chillón Geck, C., Dragos, K., and Smarsly, K. (2023). Adaptive Fault Diagnosis for Simultaneous Sensor Faults in Structural Health Monitoring Systems. Infrastructures, 8(3), 39.

Biddle, L. and Fallah, S. (2021). A novel fault detection, identification and prediction approach for autonomous vehivle controllers using SVM. Automotive Innovation, 4(3), pp. 301-314.

Cheng, X., Wang, D., Xu, C., and Li, J. (2021). A sensor fault identification method based on adaptive particle swarm optimization support vector machine. In: Proceedings of the 6th International Conference on Maintenance Engineering. Tianjin, China. October 20, 2021.

Deng, Y., Zhao, Y., Ju, H., Yi, T.H., and Li, A. (2024). Abnormal data detection for structural health monitoring: State-of-the-art review. Developments in the Built Environment, 17(2024), 100337.

Dervilis, N., Antoniadou, I., Barthorpe, R. J., Cross, E. J., and Worden, K. (2016). Robust methods for outlier detection and regression for SHM applications. International Journal of Sustainable Materials and Structural Systems, 2(1/2), pp. 3-26.

Dong, C.-Z. and Catbas, F. N. (2021). A review of computer vision-based structural health monitoring at local and global levels. Structural Health Monitoring, 20(2), pp. 692-743.

Dragos, K., Makarios, T., Karetsu, I., Manolis, G. D., and Smarsly, K. (2020). Detection and correction of synchronization-induced errors in operational modal analysis. Archive of Applied Mechanics, 90(7), pp. 1547-1567.

Dragos, K. and Smarsly, K. (2016). Distributed adaptive diagnosis of sensor faults using structural response data. Smart Materials and Structures, 25(10), 105019.

Dragos, K., Smarsly, K., and Jahr, K. (2016). Nonlinear sensor fault diagnosis in wireless sensor networks using structural response data. In: Proceedings of the 23rd International Workshop of the European Group for Intelligent Computing in Engineering. Krakow, Poland. June 29, 2016.

Fandango, A. (2018). Mastering TensorFlow 1.x: Advanced machine learning and deep learning concepts using TensorFlow 1.x and Keras. Birmingham, UK: Packt.

Fritz, H., Peralta Abadía, J. J., Legatiuk, D., Steiner, M., Dragos, K., and Smarsly, K. (2022). Fault diagnosis in structural health monitoring systems using signal processing and machine learning techniques. In: Cury, A., Ribeiro, D., Ubertini, F., and Todd, M. D. (Eds.), Structural Health Monitoring Based on Data Science Techniques. Pp. 143-164. Cham, Switzerland: Springer.

Giordano, P.F. and Quda, S. (2023). The value of monitoring a structural health monitoring system. Structural Safety, 100(2023), 102280.

Guo, Y. (2023). Sensor fault classification for bridge SHM using LSTM-based with 1D-CNN feature extraction. In: Proceedings of the 4th International Conference of Civil Architecture and Disaster Prevention and Control. Suzhou, China. March 24, 2023.

Huang, H.-B., Yi, T.-H., and Li, H.-N. (2017). Bayesian Combination of Weighted Principal-Component Analysis for Diagnosing Sensor Faults in Structural Monitoring Systems. Journal of Engineering Mechanics, 143(9), 04017088.

Isermann, R. and Ballé, P. (1997). Trends in the application of model-based fault detection and diagnosis of technical processes. Control Engineering Practice, 5(5), pp. 709-719.

Kullaa, J. (2007). Sensor fault identification and correction in vibration-based multichannel structural health monitoring. Structural Health Monitoring 2007: Quantification, Validation, and Implementation, 1(2007), pp. 606-613.

Law, K. H., Smarsly, K. and Wang, Y. (2014). Sensor Data Management Technologies for Infrastructure Asset Management. In: Wang, M. L., Lynch, J. P. & Sohn, H. (Eds.). Sensor Technologies for Civil Infrastructures. Pp. 3-32. Sawston, UK: Woodhead Publishing, Ltd.

Li, L., Luo, H., Qi, H., and Wang, F. (2023b). Sensor Fault Diagnosis Method of Bridge Monitoring System Based on FS-LSTM. In: Yang, Y. (Eds). Advances in Frontier Research on Engineering Structures. Lecture Notes in Civil Engineering. pp. 487-501. Singapore: Springer.

Li, S., Jin, L., Qiu, Y., Zhang, M., and Wang, J. (2023a). Signal anomaly detection of bridge SHM system based on two-stage deep convolutional neural networks. Structural Engineering International, 33(1), pp. 74-83.

Liu, Y. and Nayak, S. (2012). Structural health monitoring: State of the art and perspectives. Journal of the Minerals, Metals, and Materials Society, 64(7), pp. 789-792.

Luca A.V., Simon-Várhelyi, M., Mihály, N.B., and Cristea, V.M. (2023). Fault type diagnosis of the WWTP dissolved oxygen sensor based on Fisher discriminant analysis and assessment of associated environmental and economic impact. Applied sciences (Switzerland), 13(4), 2554.

Luo, Y., Wang, L., Guo, X., Zheng, J., Liao, F., and Guo, Z. (2023). Structural damage identification based on convolutional neural network group considering sensor fault. Korean Society of Civil Engineers Journal of Civil Engineering, 27(8), pp. 3403-3417.

Mou, J., Feng, L., and Qian, X. (2022). Sensor fault diagnosis using deep learning for offshore structural health monitoring. In: Proceedings of the 1st International Conference of Metrology and Digital Transformation. Berlin, Germany. September 19, 2022.

Nong, X., Luo, X, Lin, S., Ruan, Y., and Ye, X. (2023). Multimodal deep neural network-based sensor data anomaly diagnosis method for structural health monitoring. Buildings, 13(8), 1976.

Sergiyenko, O., Tyrsa, V., and Zhirabok, A. (2022). Sensor fault identification in linear and nonlinear dynamic systems via sliding mode observers. IEEE Sensors Journal, 22(11), pp. 10173-10182.

Oncescu, A.M. and Cicirello, A. (2022). A self-supervised classification algorithm for sensor fault identification for robust structural health monitoring. In: Proceedings of the 10th European Workshop on Structural Health Monitoring. Palermo, Italy, July 04, 2022.

Pan, Q., Bao, Y., and Li, H. (2023). Transfer learning-based data anomaly detection for structural health monitoring. Structural Health Monitoring Journal, 22(5), pp. 3077-3091.

Pattonn, R. J. (1990). Fault detection and diagnosis in aerospace systems using analytical redundancy. Computing and Control Engineering Journal, 2(3), pp. 127-136.

Qin, S. J. and Li, W. (1999). Detection, identification, and reconstruction of faulty sensors with maximized sensitivity. The Global Home of Chemical Engineers, 45(9), pp. 1963-1976.

Shajihan, S.A.V., Wang, S., Zhai, G., and Spencer, B.F. (2022). CNN based data anomaly detection using multi-channel imagery for structural health monitoring. Smart Structures and Systems, 29(1), pp. 181-193.

Shen, D., Yang, D., Lyo, C., Ma, J., Hinds, G., Sun, Q., Du, L., and Wang, L. (2024). Multi-sensor multi-mode fault diagnosis for lithium-ion battery packs with time series and discriminative features. Energy, 290(2024), 130151.

Smarsly, K. and Law, K. H. (2014). Decentralized fault detection and isolation in wireless structural health monitoring systems using analytical redundancy. Advances in Engineering Software, 73(2014), pp. 1-10.

Smarsly, K. and Petryna, Y. (2014). A decentralized approach towards autonomous fault detection in wireless structural health monitoring systems. In: Proceedings of the 7th European Workshop on Structural Health Monitoring. Nantes, France. July 08, 2014.

Smarsly, K., Dragos, K., and Kölzer, T. (2022a). Sensor-integrated digital twins for wireless structural health monitoring of civil infrastructure [Sensorintegrierte digitale Zwillinge für das automatisierte Monitoring von Infrastrukturbauwerken]. Bautechnik, 99(6), pp. 471-476.

Smarsly, K., Worm, M., and Dragos, K. (2022b). Design and validation of a mobile structural health monitoring system based on legged robots. In: Proceedings of the 29th International Workshop on Intelligent Computing in Engineering. Aarhus, Denmark, July 08, 2022.

Steiner, M., Legatiuk, D., and Smarsly, K. (2019). A support vector regression-based approach towards decentralized fault diagnosis in wireless structural health monitoring systems. In: Proceedings of the 12th International Workshop on Structural Health Monitoring: Enabling Intelligent Life-Cycle Health Management for Industry Internet of Things. Stanford, USA. September 10, 2019.

Taimoor, M., Lu, X., Maqsood, H., and Sheng, C. (2021). Adaptive rapid neural observer-based sensors fault diagnosis and reconstruction of quadrotor unmanned aerial vehicle. Aircraft Engineering and Aerospace Technology, 93(5), pp. 847-861.

The MathWorks, Inc. (2022). MATLAB version: 9.13.0 (R2022b), Natick, Massachusetts. Available at: https://www.mathworks.com *[Accessed January 26, 2024].*

Xia, J., Li, Z., Gao, X., Guo, Y., and Zhang, X. (2023). Real-Time sensor fault identification and remediation for single-phase grid-connected converters using hybrid observers with unknown input adaptation. IEEE transactions on industrial electronics, 70(3), pp. 2407-2418.

Yan, L., Zhang, H., Dong, X., Zhou, Q., Chen, H., and Tan, C. (2021). Unscented Kalman-filter-based simultaneous diagnostic scheme for gas-turbine gas path and sensor faults. Measurement Science and Technology, 32(9), 095905.

Yu, C.-B., Hu, J.-J., Li, R., Deng, S.-H., and Yang, R.M. (2014). Node Fault Diagnosis in WSN Based on RS and SVM. In: Proceedings of the 2014 International Conference on Wireless Communication and Sensor Network. Wuhan, China. December 13, 2014.

Zhu, L., Liu, J., Ma, Y., Zhou, W., and Yu, D. (2020). A coupling diagnosis method for sensor faults detection, isolation and estimation of gas turbine engines. Energies, 13(18), 4976.